Electronic Supplementary Material (ESI) for Nanoscale.

Supporting Information

Synthesis of Cu_3N and Cu_3N-Cu_2O Multicomponent Mesocrystals: Non-Classical Crystallization and Nanoscale Kirkendall Effect

Darinka Primc,[1,2,¶*] Luca Indrizzi,[1] Elena Tervoort,[1] Fang Xie,[2] Markus Niederberger[1]

[1]*Laboratory for Multifunctional Materials, Department of Materials, ETH Zurich, Vladimir-Prelog-Weg 5, 8093 Zurich, Switzerland.*

[2]*Department of Materials and London Centre for Nanotechnology, Imperial College London, London SW7 2AZ, United Kingdom*

Present address:

¶*Energy Storage and Distributed Resources Division, Lawrence Berkeley National Laboratory, Berkeley, CA 94720, United States*

Corresponding author: Darinka Primc*, email: dprimc@lbl.gov

1. Additional Experimental Details

Scheme S1: The schematic of the reaction setup for the synthesis of Cu_3N mesocrystals.

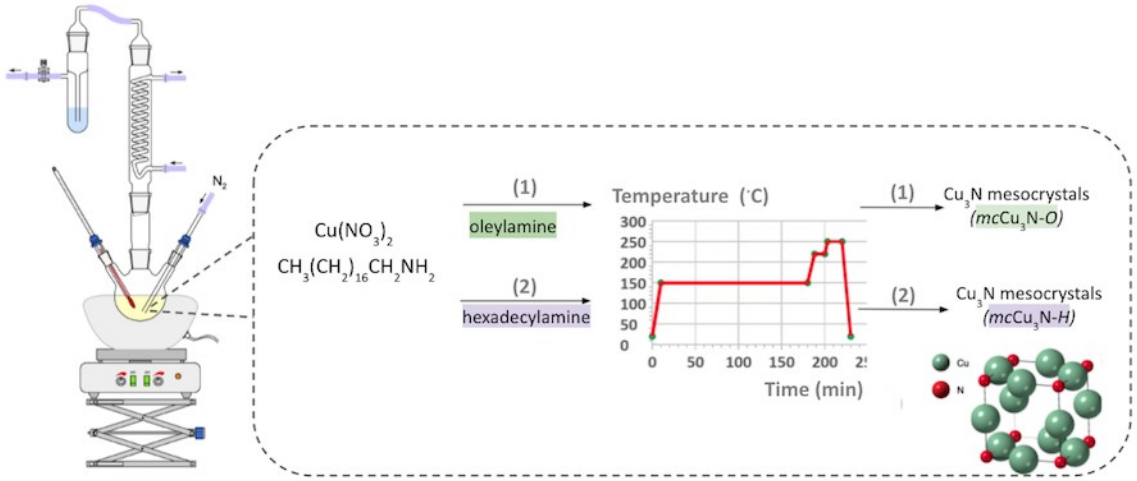

Table S1: List of Samples' Abbreviations with Corresponding Synthesis Conditions.

Sample code	Capping agent	Synthesis conditions
mcCu_3N-*O*	oleylamine	Reacted at 250 °C for 10 min.
mcCu_3N-*15*	oleylamine	Reacted at 250 °C for 15 min.
mcCu_2O-*20*	oleylamine	Reacted at 250 °C for 20 min.
mcCu_2O-*30*	oleylamine	Reacted at 250 °C for 30 min.
mcCu_3N-*H*	hexadecylamine	Reacted at 250 °C for 10 min.
mcCu_3N-Cu_2O-*20*	hexadecylamine	Reacted at 250 °C for 20 min.
mcCu_3N-Cu_2O-*25*	hexadecylamine	Reacted at 250 °C for 25 min.
mcCu_3N-Cu_2O-*30*	hexadecylamine	Reacted at 250 °C for 30 min.
intCu_3N-*O*	oleylamine	Intermediate product corresponding to the early stages of *mc*Cu_3N-*O*, sampled at 220 °C
intCu_3N-*H*	hexadecylamine	Intermediate product corresponding to the early stages of *mc*Cu_3N-*H* sampled at 250 °C after 1 min.

2. Synthesis of mesocrystals

2.1. Additional TEM/XRD/SAED analysis of *mc*Cu_3N-*O*

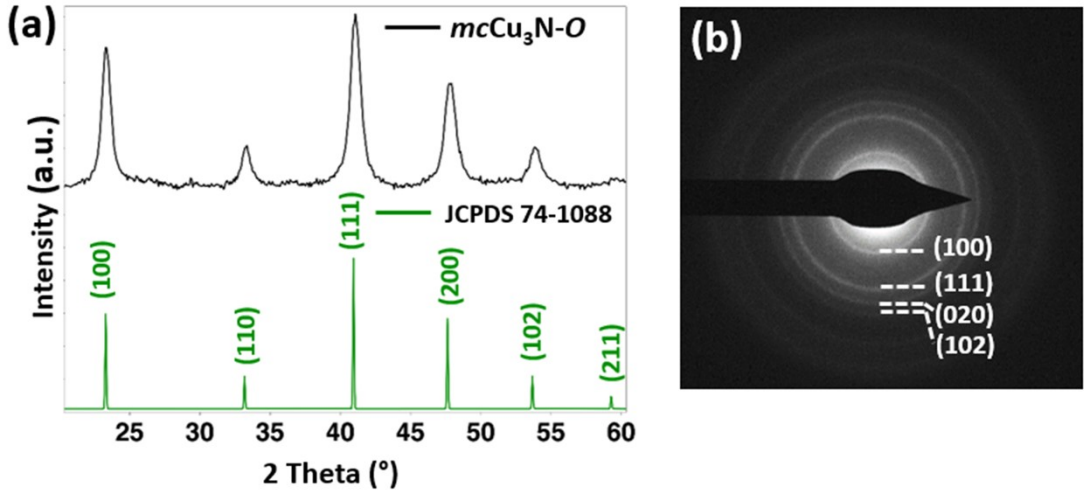

Figure S1: X-ray diffraction pattern of *mc*Cu_3N-*O* (a), and SAED (b) recorded over representative area in Figure 1a, confirming anti-ReO_3 structure (JCPDS # 074-1088) of nanocrystalline Cu_3N. The size of crystallites estimated from peak broadening of (100) reflection at 23 ° using Scherrer equation is 8.5 nm.

2.2. Energy dispersive X-ray spectroscopy of *mc*Cu_3N-*O*.

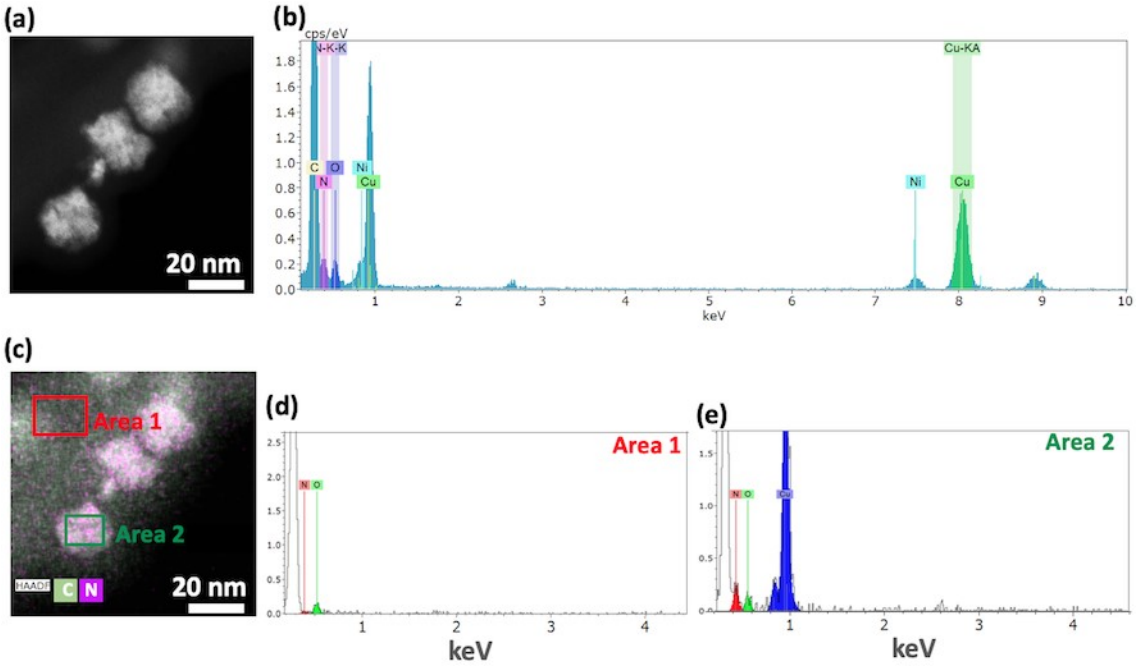

Figure S2: Spectrum image with corresponding EDS spectra (a-b). The HAADF signal shows the *mc*Cu_3N-*O* particles at the edge of the supporting material (a), and the corresponding EDS spectrum (b) from the region in (a). The C-K, N-K and O-K signals in the spectrum are also due to the conventional TEM support foil material. HAADF-STEM of (a) with the color overlay of N-K and C-K signals with two marked regions for the extracted EDS spectra within (d) and outside (e) of the particle volume.

2.3. Additional TEM/XRD/SAED analysis of *mc*Cu_3N-*H*

2.3.1 X-ray diffraction of *mc*Cu_3N-*H*.

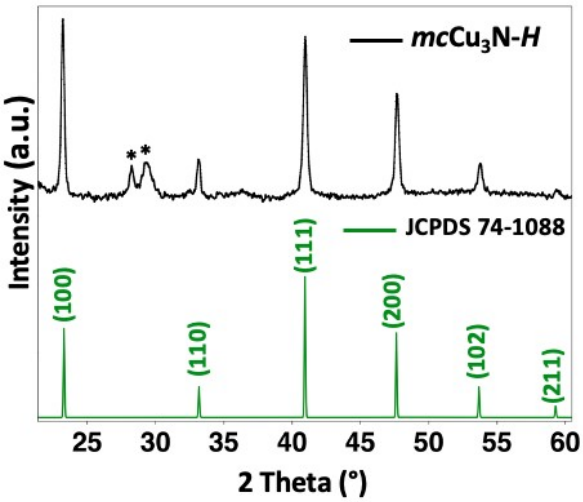

Figure S3: X-ray diffraction pattern of *mc*Cu_3N-*H,* confirming anti-ReO_3 structure (JCPDS # 074-1088) of nanocrystalline Cu_3N. The reflections at 28° and 29 ° correspond to the residual precursor. Time-depend XRD study of *mc*Cu_3N-*H* (Figure 5, sample *mc*Cu_3N-Cu_2O-*20*) reveals that under longer reaction time, the signal at 29° disappears.

2.3.2. Additional TEM/SAED analysis of *mc*Cu_3N-*H*

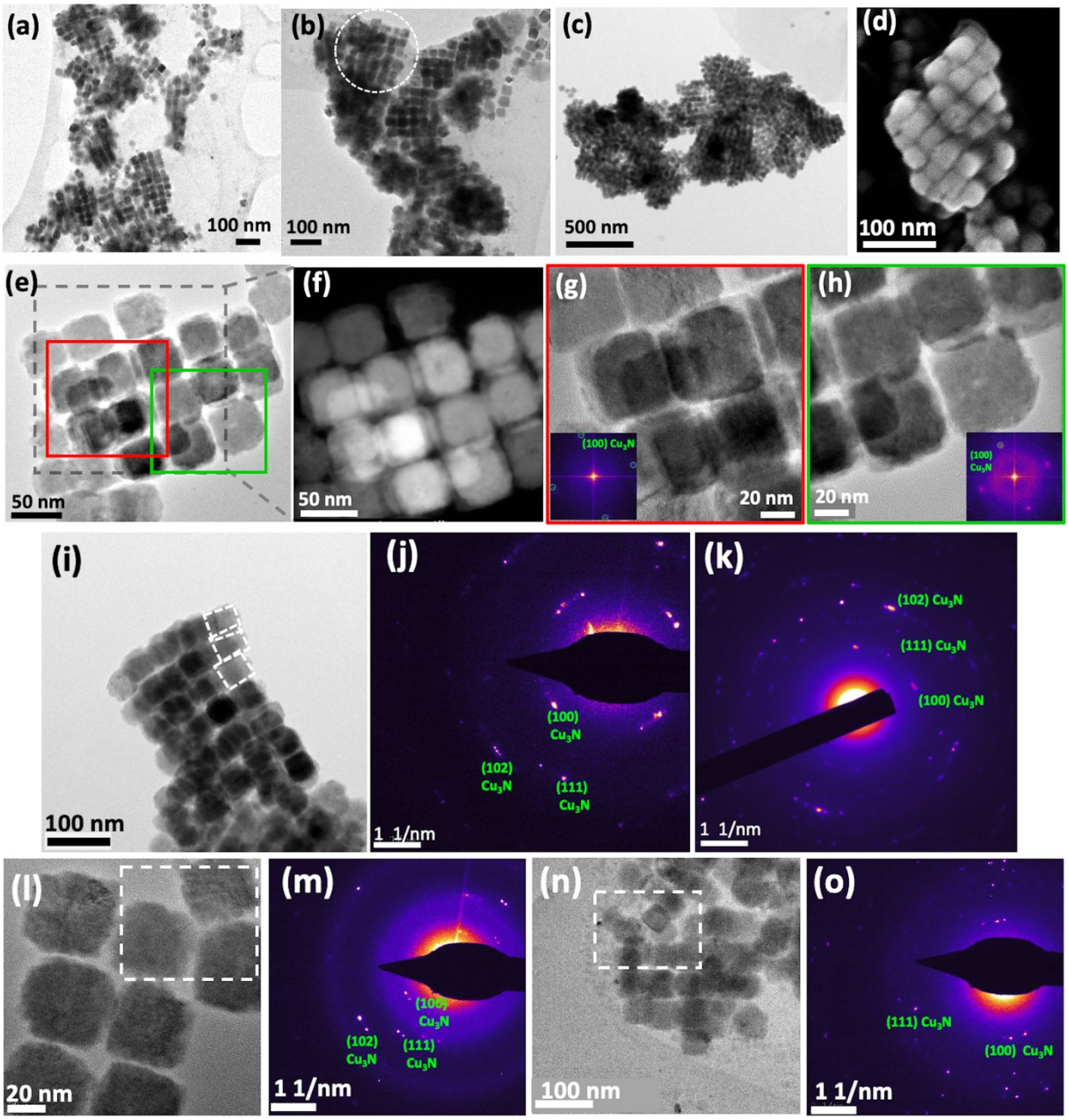

Figure S4: TEM micrographs showing random size/morphology of the mesocrystals in *mc*Cu_3N-*H* (a-b). Seldomly observed, mesocrystals in *mc*Cu_3N-*H* form larger µm-sized aggregates (c). FESEM (d), TEM (e) and STEM micrograph (f) showing examples of overlayed subunits in *mc*Cu_3N-*H*. The overlayed subunits of areas highlighted in red and green squares in (e) are displaying translational and rotational order, which is depicted with the corresponding FFTs in panels (g) and (h). The example of the slightly distorted orientational order of subunits of one mesocrystal (marked with doted white squares), in panel (i), with the corresponding

texture-like SAED (j). SAED (k) of the area marked with dotted circle in panel (b). Similar observations of slightly distorted mesocrystals with orientational relations and atomistic models, are reported in the literature for mesocrystals of magnetite (Fe_3O_4)[1,2] and PbS[3,4]. TEM/SAED analysis of *int*Cu_3N-*H* ; SAED (m) of the TEM in panel (l) showing face-to-face attachment, and SAED (o) of the area marked with circle in (n) indicating edge-to-face attachment.

2.3.3. Energy dispersive X-ray spectroscopy of *mc*Cu_3N-*H*.

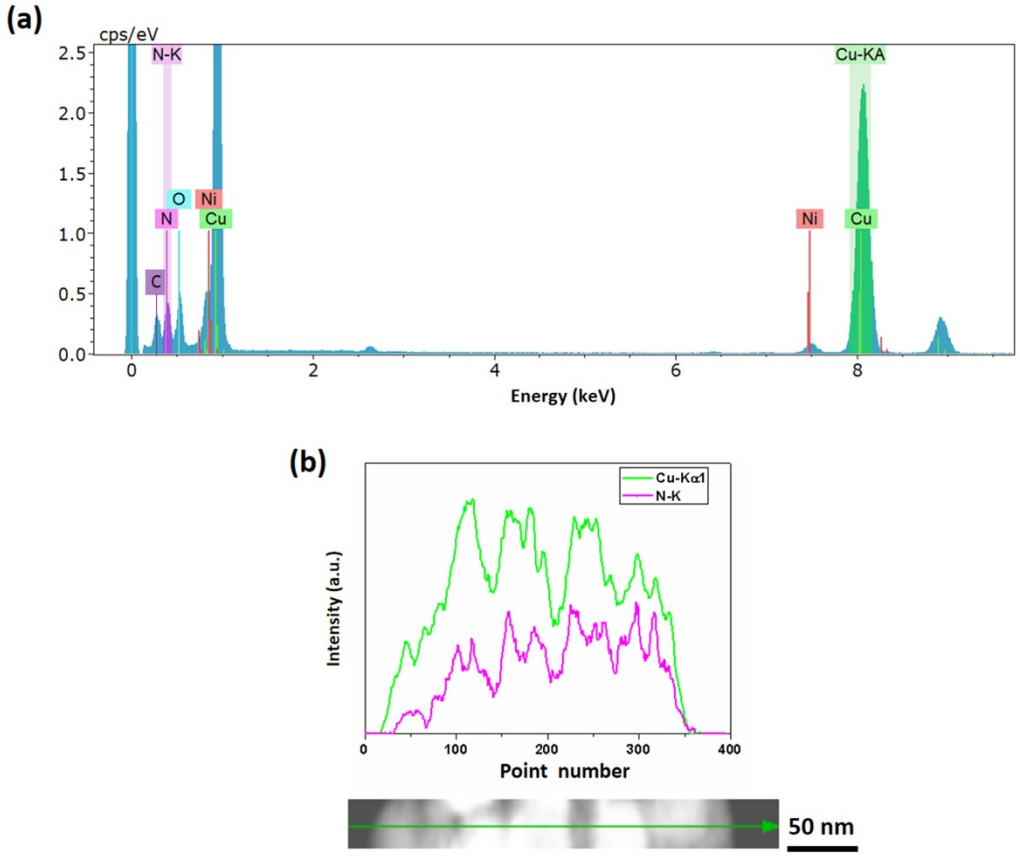

Figure S5: EDXS spectra of *mc*Cu_3N-*H* recorded over the HAADF-STEM area of Figure 2b shows the presence of N and Cu (a). The signal for Ni, C and O are originating from the TEM specimen support. Intensity profile analysis showing elemental distribution along several adjacent overlayed subunits in a line scan mode of EDS STEM from *mc*Cu_3N-*H* mesocrystal region, depicting the distributions of Cu-K (green) and N-K (pink) signal (b).

3. Attachment modes of subunits in mesocrystals

3.1. *Attachment modes of subunits in mc*Cu_3N-*O mesocrystals*

A combination of TEM (Figure 1b, Figure S6a-f,) and STEM images (Figure 1a, Figure S6g-i inset) is used to assess the mutual crystallographic alignment of nanosized subunits in *mc*Cu_3N-*O*. Throughout analysis of *mc*Cu_3N-*O*, encompassing over 30 HRTEM/FFT patterns shows that subunits of mesocrystals are always aligned in crystallographic register.

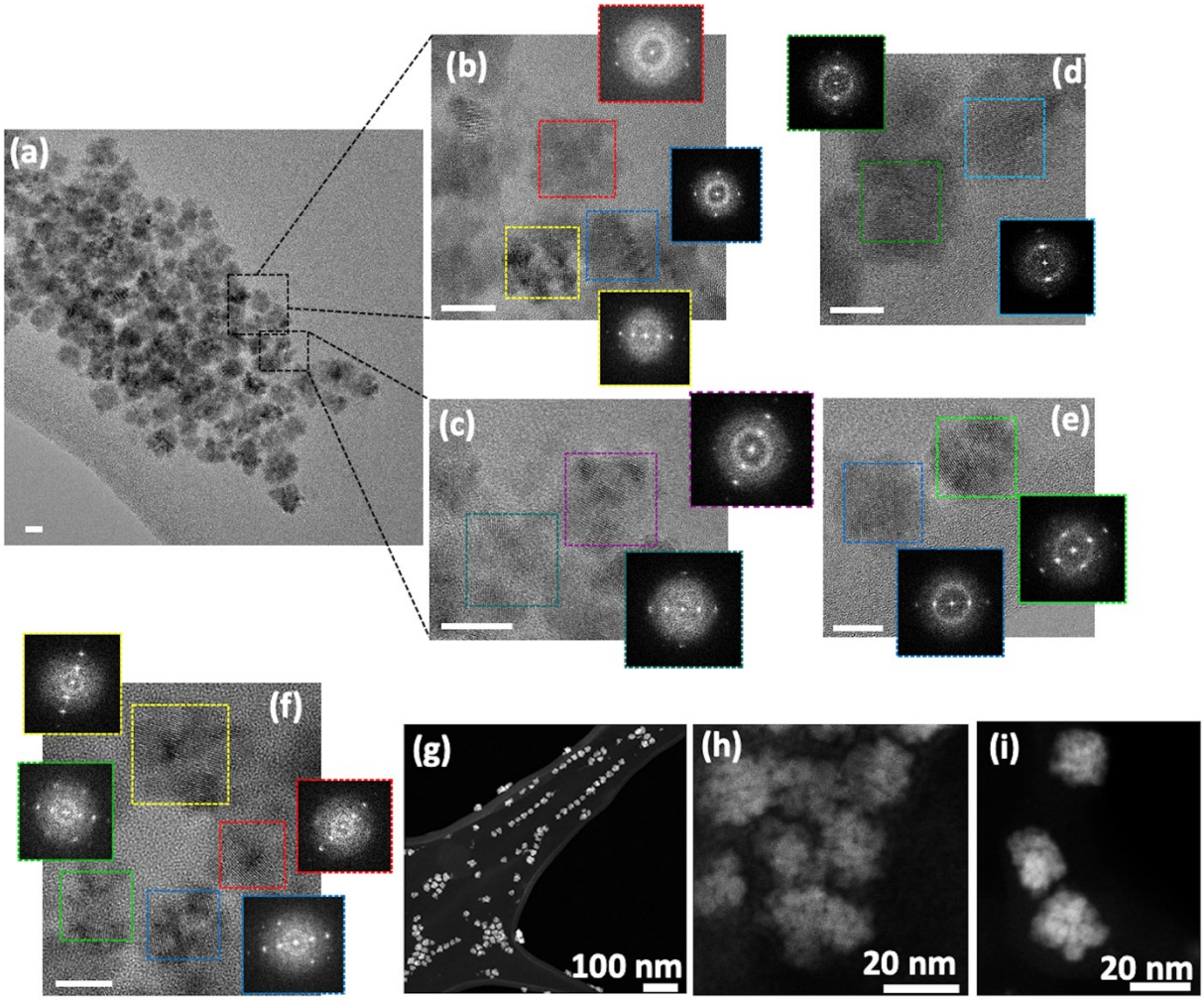

Figure S6: TEM micrographs of the area shown in Figure 1a (a) with combined HRTEM/FFT patterns of several mesocrystals of *mc*Cu_3N-*O* (b-f), showing that individual mesocrystals are composed of partially connected faceted subunits with the corresponding FFTs depicting their mutual crystallographic orientation. STEM micrographs showing porosity of mesocrystals in *mc*Cu_3N-*O* (g-i). Scale bars in (a-f) correspond to 10 nm.

3.2. Analysis of the early reaction stages.

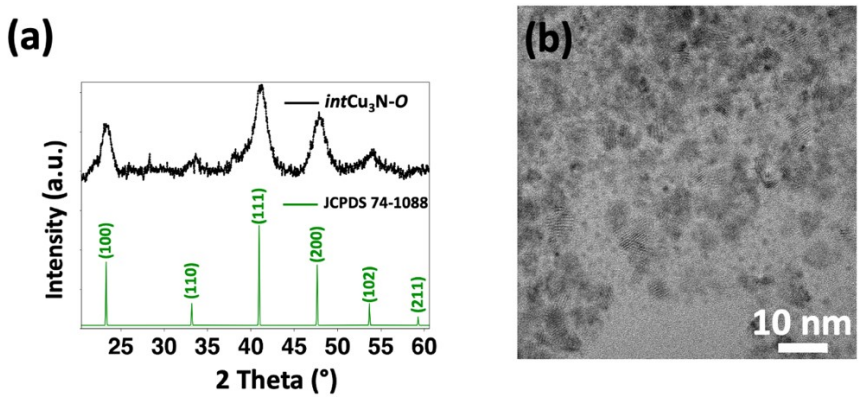

Figure S7: The XRD pattern of a sample obtained after heating a solution of precursors containing oleylamine at intermediate temperature of 220 °C (*int*Cu_3N-*O*) confirming the formation of nanocrystalline Cu_3N with the crystallite size of 4.5 nm determined from peak broadening of (100) reflection using Scherrer equation (a). TEM micrograph of a sample *int*Cu_3N-*O* (b).

3.3. Attachment modes of subunits in *mc*Cu_3N-*H* mesocrystals

The analysis of binding pathways of the subunits occurring in *mc*Cu_3N-*H* is gained by analyzing the attachment modes of nanoparticles, i.e. mesocrystals' subunits of an intermediate product (*int*Cu_3N-*H*) and the final products (*mc*Cu_3N-*H*). Results, assessed in > 80 TEM micrographs, presents the analysis of 119 subunits of intermediate, and 101 subunits of the final product.

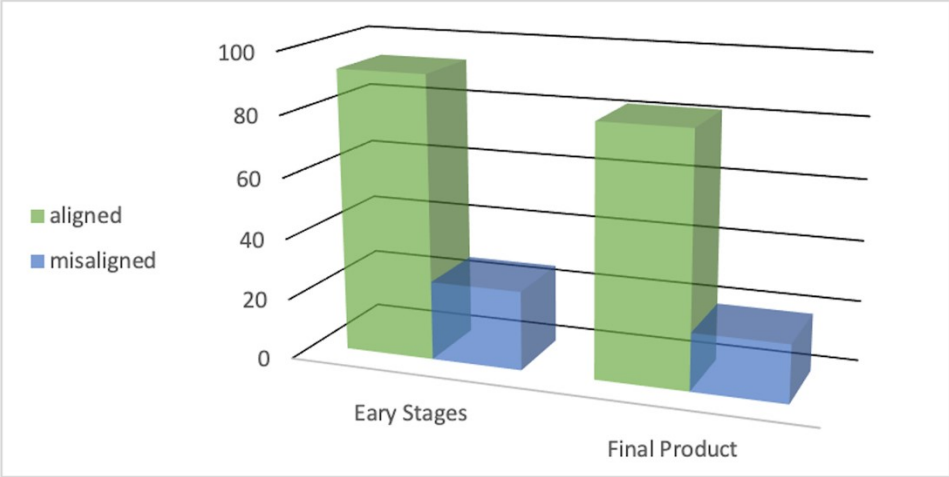

Figure S8: Graph presenting number of crystallographically aligned (green) and misaligned (blue) attachments detected in the early reaction stages *(int*Cu_3N-*H)* in comparison to the number of aligned (green) and misaligned (blue) attachments in the final product (*mc*Cu_3N-*H)*. The differences in aligned attachments in the early stages (78% in *int*Cu_3N-*H*), compared to those in the final product (81% in *mc*Cu_3N-*H*) are negligible, suggesting that after subunits come into contact through misaligned attachment, they only rarely rotate into aligned face-to-face configuration.

4. Chemical Conversion

4.1. *Chemical conversion of mcCu_3N-O into Cu_2O hollow structures.*

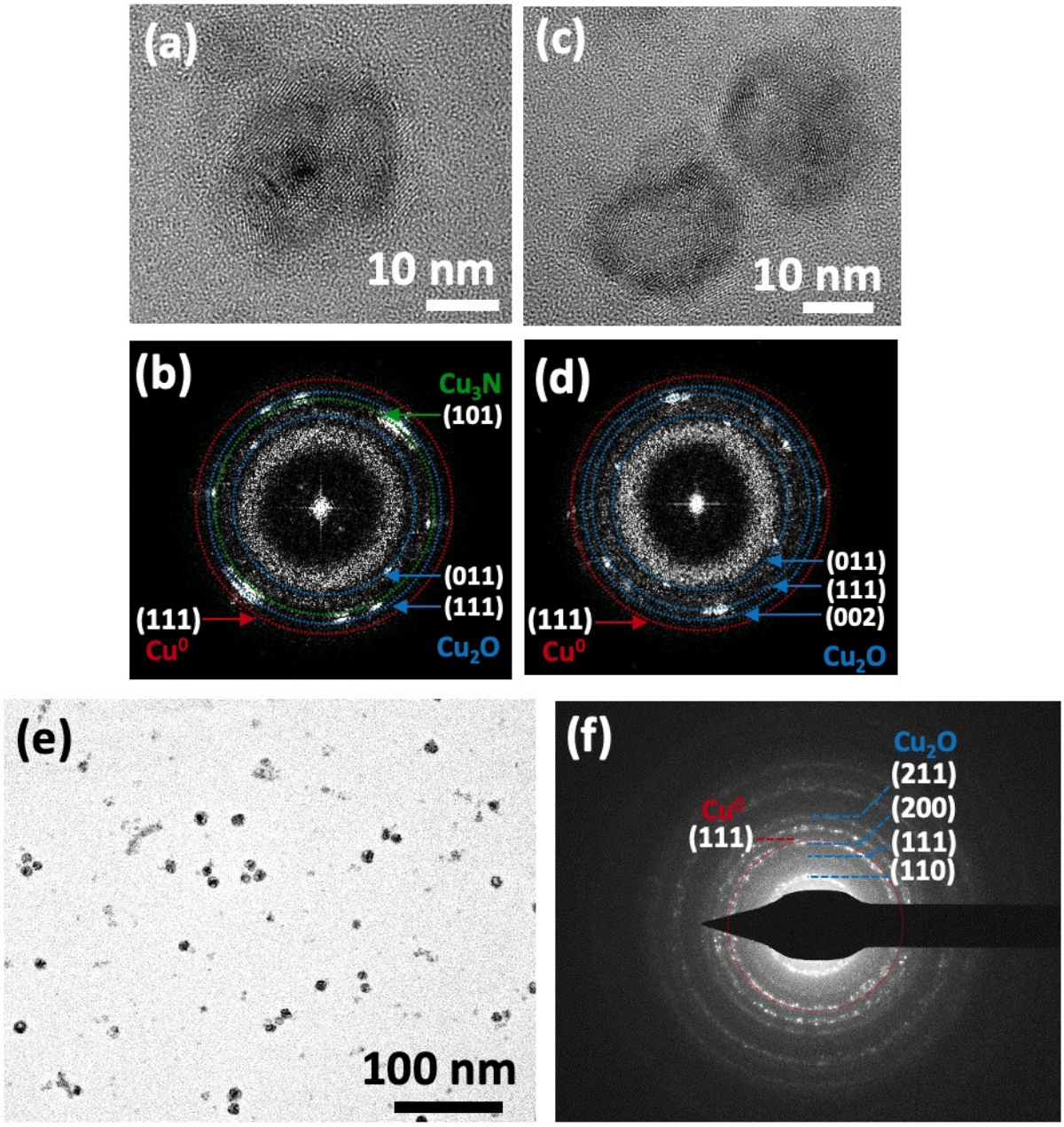

Figure S9: Combined HRTEM/FFT analysis depicts the morphology of two types of structures detected in the sample *mc*Cu_3N-*15:* Cu_3N mesocrystal that partially converts to Cu/Cu_2O (a-b) and hollow nanoparticles of mixed Cu and Cu_2O phases (c-d). An overview TEM image of nanocages of *mc*Cu_2O-*30* (e), and the corresponding SAED recorded over the area in (e) revealing the presence of cubic Cu_2O and metallic Cu.

4.1.1. *EDXS spectra of mc*Cu_2O-*30*

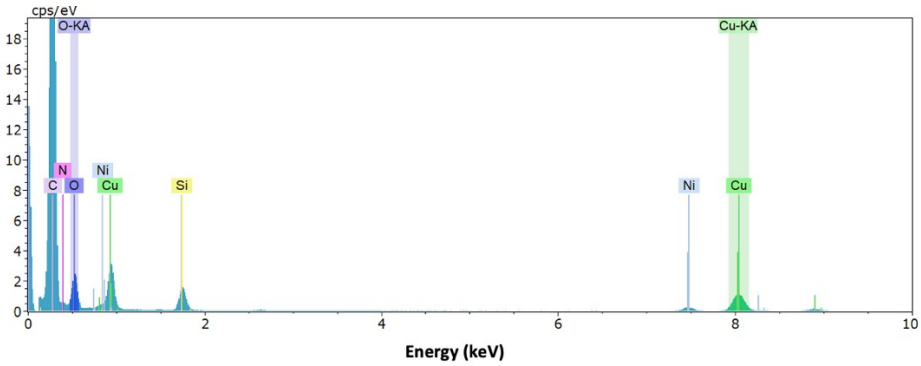

Figure S10: The EDXS analysis of hollow nanoparticles of *mc*Cu_2O-*30*, showing the presence of Cu and O, and the absence of N signal. The signals of Si, Ni and C are originating from the TEM specimen support. The EDXS analysis of *mc*Cu_2O-*20*, is complemented by the XRD (Figure 4a) and HRTEM/FFT data (Figure 4c-d, Figure S9c-f, Supporting Information).

4.2. Chemical conversion of *mc*Cu_3N-*H* into Cu_3N-Cu_2O multicomponent mesocrystals.

4.1.2. *EDXS spectra and EDXS line analysis*

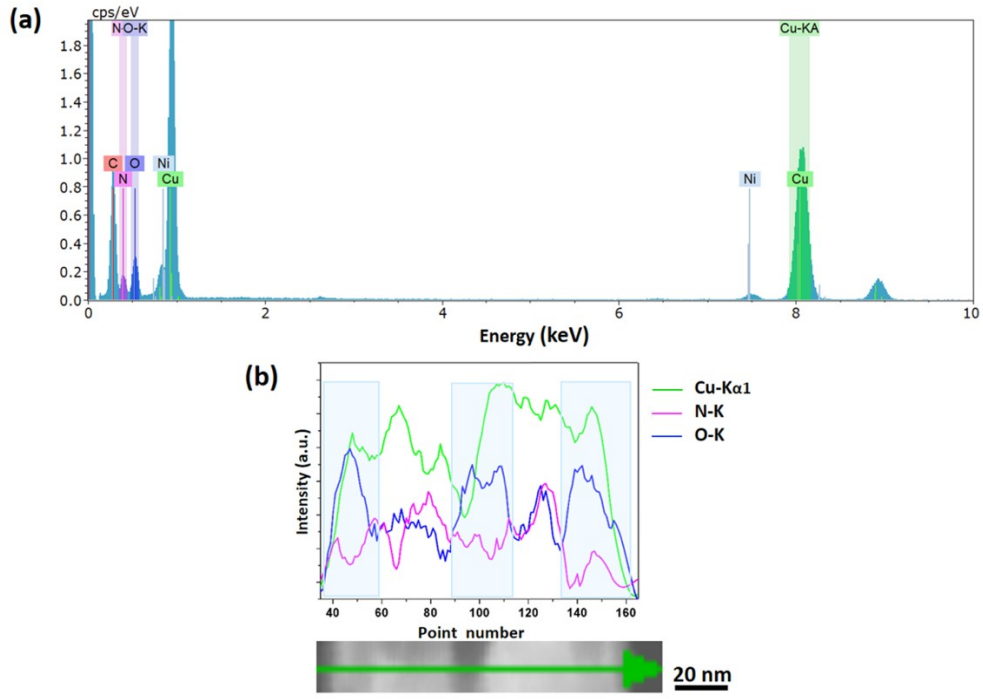

Figure S11: EDXS spectra of a *mc*Cu_3N-Cu_2O-*20* showing elemental distribution over the representative area of one mesocrystal of Figure 6a (a). Signals for Ni and C are originating from TEM specimen support. Intensity profile analysis showing the elemental content

distribution across two adjacent subunits acquired in a line scan mode of EDS STEM from a *mc*Cu_3N-Cu_2O-*20* mesocrystal region (b). Light blue bars highlight the increase of the O-K signal (blue) compared to the N-K signal (pink) at the edges of the subunits. For the line-scan analysis smoothing over 5 pxl was performed by the Savitzky-Galay method.

References:

1 J. Brunner, I. A. Baburin, S. Sturm, K. Kvashnina, A. Rossberg, T. Pietsch, S. Andreev, E. Sturm (née Rosseeva) and H. Cölfen, *Adv. Mater. Interfaces*, 2017, **4**, 1600431.

2 Z. Quan, H. Xu, C. Wang, X. Wen, Y. Wang, J. Zhu, R. Li, C. J. Sheehan, Z. Wang, D.-M. Smilgies, Z. Luo and J. Fang, *J. Am. Chem. Soc.*, 2014, **136**, 1352–1359.

3 C. Schliehe, B. H. Juarez, M. Pelletier, S. Jander, D. Greshnykh, M. Nagel, A. Meyer, S. Foerster, A. Kornowski, C. Klinke and H. Weller, *Science (80-.).*, 2010, **329**, 550 LP – 553.

4 P. Simon, E. Rosseeva, I. A. Baburin, L. Liebscher, S. G. Hickey, R. Cardoso-Gil, A. Eychmüller, R. Kniep and W. Carrillo-Cabrera, *Angew. Chemie Int. Ed.*, 2012, **51**, 10776–10781.